Analyst

TUTORIAL REVIEW

View Article Online
View Journal | View Issue

Cite this: *Analyst*, 2026, **151**, 11

A practical guide to working with nanopipettes

Dominik Duleba, Adria Martínez-Aviñó and Robert P. Johnson *

Nanopipettes are a powerful solid-state nanopore platform with applications including single-particle characterization, surface mapping, and high-sensitivity analytical measurement in both bulk solutions and in localized spaces. While the capabilities of the platform have been aptly demonstrated, practical challenges associated with the nanopipette fabrication, filling, and surface modification remain. Progress and advancement to a high device readiness level are also hindered by low reproducibility and low throughput, as well as the consequent entry barrier for new research groups. This perspective provides the accumulated practical experience of our research group, forming a practical guide to overcoming the technical hurdles that are rarely discussed within the primary literature. We outline fabrication protocols, namely the importance of environmental conditions and instrument maintenance for enhanced reproducibility, as well as the desirable nanopipette geometries to facilitate ease of filling and surface modification. Filling procedures are discussed, and the interplay of surface wetting, capillary forces, and surface chemistry is used to understand how filling issues might be mitigated. Silanization of nanopipettes as a route for surface modification of the nanopipette interior is also discussed, with a particular focus on vapor-phase silanization. General design principles for surface grafting reactions are offered to maximize throughput and reproducibility. Throughout the perspective, the interconnected nature of the fabricated geometry, filling, and the modification pathways are highlighted, and this perspective is meant to facilitate the design of a holistic workflow where each stage is considered in tandem, facilitating higher throughput and more reproducible nanopipette research.

Received 24th October 2025,
Accepted 26th November 2025

DOI: 10.1039/d5an01128k

rsc.li/analyst

Nanopores have been utilized in a number of exciting applications including high-sensitivity analyte detection,[1,2] particle counting and characterization,[3–5] and DNA-sequencing.[6–8] Although early nanopore research has predominantly utilized biological pores assembled in lipid bilayers,[9,10] the need for more physically and chemically robust and tuneable platforms has increased research intensity into solid-state nanopores.[11–13] Solid-state nanopores are typically fabricated in thin polymer membranes using focused ion/electron beams,[13] chemical etching,[14] or, more recently, controlled dielectric breakdown.[15] These fabrication methods, however, often suffer from low throughput and produce nanopores that are embedded within a macroscopic membrane with highly limited spatial control of the nanopore position, limiting their utility as spatially controllable probes.

The desire for higher spatial precision, higher throughput, and the subsequent ability to use nanopores as scanning probes has led to the widespread adoption of nanopipettes.[16–18] Nanopipettes consist of glass capillaries that taper to needle-like conical geometries terminating in a single, well-defined nanopore. Their rigid, needle-like geometry makes them ideally suited for scanning probe applications, such as Scanning Ion Conductance Microscopy (SICM),[19–21] and enables their use as sensors capable of highly localized measurements through direct insertion into cells or other spatially constricted analyte environments.[22–24] Although nanopipettes are uniquely suited for probe-based and localized measurement applications, nanopipettes retain full compatibility with bulk solution measurements and have found extensive use in analytical chemistry applications[25] (Fig. 1).

The utility of nanopipettes stems from the unique electrokinetic behaviors that arise due to the nanoconfined ion transport at the tip region. In Coulter-type particle counting applications (resistive pulse sensing), the entry of particles into the nanoscale aperture displaces a significant fraction of the available ions, resulting in decreased pore conductance and a measurable ion current drop.[26,27] In another analytical method, ion current rectification sensing exploits the overlapping electric double layers, which impose ion selectivity and generate a characteristic diode-like electrical response.[28–31] The immobilization of charged analytes onto the nanopipette surface through analyte-specific probe molecules modulates the electric double layer and leads to a detectable change in the diode-like behavior, forming the basis for quantitative

School of Chemistry, University College Dublin, Belfield, Ireland.
E-mail: robert.johnson@ucd.ie

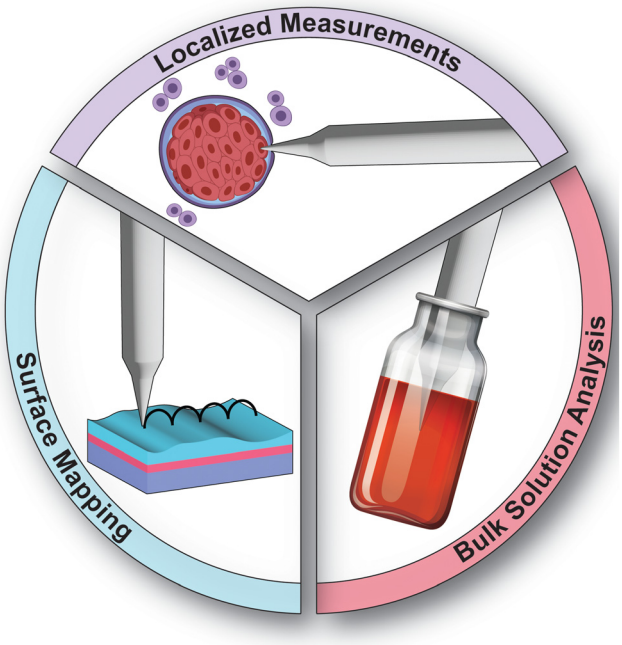

Fig. 1 The common approaches in which nanopipettes can be utilized.

measurements.[2] While the sensitivity and utility are enabled by these nanoconfined transport phenomena and the needle-like geometry, they also impose substantial practical challenges.

Despite the growing popularity of nanopipette-based research and the publication of many exciting applications and fundamental studies, the practical difficulty of working with nanopipettes remains a significant bottleneck for the field. Various practical challenges that are seldom discussed—including reproducible fabrication, pore blockage prevention, reliable filling procedures, and contamination control—hinder research efficiency in active laboratories and present a formidable entry barrier for new researchers. This perspective summarizes our accumulated experience in nanopipette fabrication, filling, and surface modification, providing detailed practical guidance for both established research groups as well as newcomers to the field. Through the inclusion of numerous troubleshooting approaches and technical recommendations, we aim to facilitate higher throughput experimental workflows and improved data quality across the nanopipette research community.

1. Fabrication of nanopipettes

Nanopipettes can be fabricated from glass capillaries using a pipette puller, such as the Sutter-P2000. A CO_2 laser melts the capillary, and its two halves are mechanically pulled apart, resulting in the controlled tapering of the molten glass and its eventual separation into two nanopipettes. The critical geometric parameters of the nanopipette—including the nanopipette's radius, cone angle, and the wall thickness, as well as the macroscale shape, taper, and length of the pipette neck—are controlled through the laser's intensity, duration, scanning pattern, as well as the timing and force of the mechanical pull. These are controlled through the five instrumental parameters of the HEAT, FILAMENT, VELOCITY, DELAY, and PULL. The HEAT defines the intensity of the laser, the FILAMENT is its scanning pattern, and the VELOCITY defines the threshold velocity the melting glass must reach for the laser to turn off. Following this, the DELAY parameter prescribes the waiting time between laser turn-off and the commencement of the hard pull, whose force is set by the PULL parameter. In general, higher HEAT, VELOCITY, and PULL values yield nanopipettes with smaller pore radii. The outer and inner diameters of the glass capillary are also a crucial consideration for program development, as well as the resulting nanopipette. In our experience, capillaries with a 1 mm outer diameter and 0.7 mm inner diameter are highly versatile, and can be used to fabricate both the sub-10 nm, as well as larger 300–500 nm nanopipettes.

1.1. Pipette puller programs

The combination of instrumental parameters that reproducibly produces nanopipettes with the desired nanopore and taper geometry is specific not only to the individual instrument but also to the environmental conditions under which the instrument is operated. As such, a new instrument in a new laboratory requires program development from scratch, and literature-reported programs must be tuned and optimized for the individual instrument and specific laboratory conditions. Fabrication programs can either be a one-line program—where the capillary is melted and separated in a single loop—or a multi-line program that performs multiple heating sequences before the capillaries separate.

In our experience, two-line programs are the most reliable and reproducible for fabricating nanopipettes with a pore radius in the 20 nm to 150 nm range; however, two-line programs fabricating sub-10 nm pores have also been reported.[32] In a two-line program, the first heating cycle melts the capillary, but the subsequent hard pull does not separate it into two nanopipettes. This first heating cycle's role is to shape the neck of the pipette. In the next heating cycle, the laser further melts and shapes the neck of the nanopipette, and then a hard pull separates the capillary to produce the nanopipettes. This two-line approach not only offers high reproducibility of the pore radius (as reproducible as 8% RSD), but also shorter and steeper neck tapers that facilitate subsequent filling. An example of such a program is provided in Table 1. This program can most easily be tuned to suit an individual instrument by adjusting the HEAT values until a heat-on time of approximately 4.6 seconds is obtained.

One-line programs are most effective for fabricating nanopipettes with pore radii below 20 nm or above 150 nm. In our experience, one-line programs are less reproducible than two-line programs, yielding higher pore-to-pore variance (≈20% RSD). A one-line program shapes the neck of the nanopipette

Table 1 A two-line program that can be adapted to fabricate a nanopipette with a pore radius of around 60 nm, as well as two one-line programs that can fabricate nanopipettes with 6 nm and 250 nm pore radii. These programs are suitable for filamented and non-filamented capillaries with an outer diameter of 1 mm and an internal diameter of 0.7 mm

Radius (nm)		Heat	Filament	Velocity	Delay	Pull
~60	Line 1	700	4	20	170	0
	Line 2	680	4	50	170	200
~6	Line 1	750	4	40	135	180
~250	Line 1	575	3	60	128	100

in a single heating event, typically producing longer and more gradual tapers that can make filling challenging. Table 1 also provides examples of one-line programs, and these can also be adjusted to an individual instrument by tuning the HEAT value until a consistent heat-on value is obtained.

1.2. Reproducible nanopipette fabrication

Beyond the development of a pipette puller program that fabricates nanopipettes with the desired pore radius and taper geometry, the geometric consistency and reproducibility of the nanopipette are equally crucial towards the development of nanopipette applications. Aside from the fabrication program, several other factors can influence fabrication reproducibility. The proper setup of the instrument is crucial, especially the alignment of the scanning mirror, which can be verified using a burn-test where a heat-sensitive paper is placed behind the capillary, and the symmetry of the burn mark reflects the mirror alignment quality. The alignment of the retro-mirror is also crucial, but this should not be changed unless all other avenues have been explored, and even then, only with a thorough consultation with the manufacturer. Most importantly, instrument cleanliness in fabrication reproducibility is vastly underestimated. Weekly cleaning (using isopropyl alcohol and lint-free tissue) of both the retro-mirror and the pulley system will significantly improve reproducibility. The capillaries should also be cleaned immediately prior to pulling. We have also found that cross-tightening of the capillary into the instrument, as well as tightening with the minimal possible force, can also improve reproducibility by avoiding uneven stress across the melting capillary. It is also good practice to warm up the instrument by turning it on at least 30 minutes before use, as well as to discard the initial pulls of each session. These initial pulls are usually of poor quality, and the reproducibility of nanopipettes increases further into the pulling session (Fig. 2). As a quality control screening process, the heat-on time of each pull can be monitored, with pulls deviating more than 0.2 seconds from the average considered as defective nanopipettes that are discarded.

We have found that environmental factors exert a high influence on the pulling process, and fluctuations in the ambient temperature and humidity can greatly affect geometric reproducibility (especially between pulls at different times of the day, different days, and seasons). Consistent timing of fabrication, such as consistently fabricating nanopipettes only in the early morning, can help minimize the impact of these fluctuations.

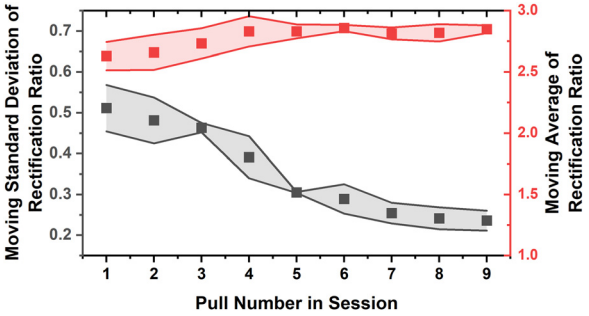

Fig. 2 The improvement in reproducibility of the rectification ratio (|*I*(−0.4 V)/*I*(+0.4 V)|) as the pulling session continues. The moving standard deviation and average are calculated with a 6 pull window size (*i.e.*, pull number 9 uses pull numbers 9–15). Three pull sessions of 15 pulls are used. The 6 nm program is used (Table 1).

2. Filling nanopipettes

Once nanopipettes have been fabricated, they will need to be filled with a solution, such as an electrolyte to enable electrochemical measurements, or with a surface grafting solution to modify the interior surface. In both cases, the nanopipettes must be filled completely with both the macro-size neck and the nano-sized tip fully wetted, and air bubbles absent. This can be challenging, especially when the neck taper is less than ideal—such as with nanopipettes that have long, narrow, and shallow tapers—or when working with nanopipettes that have been modified with hydrophobic/hydrophilic surface chemistries that make wetting difficult.

The most straightforward approach to filling a nanopipette is backfilling, where a needle, such as MicroFil Flexible needle (World Precision Instruments, MF34G-5), is used to fill the solution into the interior of the nanopipette. Counterintuitively, optimal filling is achieved not by placing the solution directly into the taper of the nanopipette, but rather into the non-melted capillary section approximately 0.5 cm away from the onset of the taper (Fig. 3A). This will result in surface wetting and capillary forces drawing the solution into the narrow-tapered region, filling the nanopipette up from the tip-end in approximately 5–20 minutes, depending on taper geometry (Fig. 3B and C). Filling in this way typically leaves a single, large air bubble at the start of the taper that can be easily removed with a syringe (Fig. 3D). Conversely, direct injection into the taper often results in numerous small air bubbles trapped inside the narrow-tapered neck that are extremely difficult or impossible to remove with a syringe. An alternative approach is to mount the partially filled nanopipette into a 3D-printed centrifuge holder and use the centrifugal force to aid wetting and nanopipette filling.[33] These filling

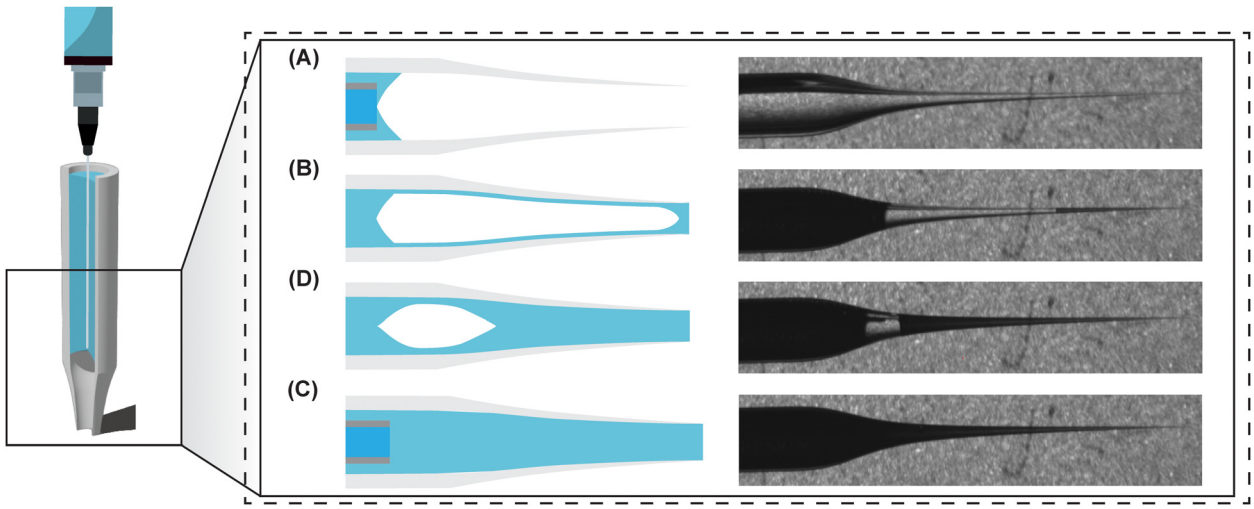

Fig. 3 A schematic illustration of how to fill a nanopipette. (A) shows that the solution is backfilled around 0.5 mm away from the start of the taper. (B) shows that capillary forces then pull the liquid into the tip, and (C) shows that over a few minutes the nanopipette fills from the tip end, leaving a single large air bubble at the start of the taper. (D) This air bubble can then be easily removed with a syringe. This method works best for a filamented nanopipette.

methods work especially well if the capillary is filamented, but can also work with non-filamented capillaries (*e.g.*, Sutter Instruments #100-70-7.5), depending on the geometry, as well as on the surface and the solution properties.

Although non-filamented capillaries can often be simply filled, sometimes the choice of solvent, electrolyte or the nanopipette geometry results in failure of the simple backfilling method described above. In this case, we have found the hot-plate method highly successful.[34] In the hot-plate method, the solution is placed as close to the tapered neck as possible, and the nanopipettes are placed on a hot plate with their tips extending beyond the heating block (Fig. 4). The hot plate is set a few degrees below the solution's boiling point (*i.e.*, 90 °C for aqueous solutions). As the tip extends beyond the heating block, and its surface-area-to-volume ratio increases as it tapers down into a nanopore, a temperature gradient is established along the length of the nanopipette, with the furthest and narrowest part of the tip being the coolest. This temperature gradient drives the repeated evaporation of solutions in the wider and hotter parts of the nanopipette, and condensation in the narrower and colder parts, gradually transporting solution towards the nanoscale aperture over a period of 30–60 minutes. Once the nanopipettes are completely filled, the electrolyte solution within the non-tapered regions of the nanopipette is replaced with fresh solution. This helps mitigate the issue of an evaporation-caused increase in the electrolyte concentration, especially in more volatile non-aqueous solvents. The hot-plate method is most effective for non-filamented capillaries, as the filament can disturb the evaporation and condensation, leading to small air bubbles trapped in the taper.

2.1. Dealing with air bubbles

Sometimes, stubborn air bubbles can remain in the narrow taper region of the nanopipette. While a nanopipette with persistent air bubbles is perhaps best discarded, they can sometimes be recovered. Some air bubbles can be mechanically dislodged with a syringe. The syringe needle is firmly pushed into the tapered neck to create a seal, and either a positive pressure or a vacuum is applied before the seal is intentionally broken through the rapid withdrawal of the syringe from the taper. Repeating this pressure-release cycle can gradually move and eventually fully dislodge the trapped air bubbles. Alternatively, the unpulled part of the nanopipette can also be gently tapped against a hard edge, and this can dislodge less stubborn air bubbles. Placing the nanopipette back onto the hotplate can also potentially remove the air bubbles, particularly for filamented capillaries, where a hot plate is not typically used for the filling process initially.

Persistent trapped air bubbles that cannot be resolved can be indicative of more fundamental problems associated with the nanopipette geometry. Tuning of the surface hydrophobicity/hydrophilicity (*via* surface functionalization), or adjusting the taper so that it is shorter and steeper, may be needed to facilitate good filling and mitigate the problem of stuck air bubbles.

3. Surface modification of nanopipettes

For many nanopipette applications, surface modification of the internal surface is necessary to enhance analytical performance or impart specific functionality. Such modifications may serve to tune the residence time of translocating species for improved sensitivity in resistive pulse sensing,[35–37] or to graft probe molecules that confer analyte-specificity in ion current rectification sensing.[38,39] Both quartz and borosilicate glass nanopipettes present oxide-based surfaces rich in Si–OH

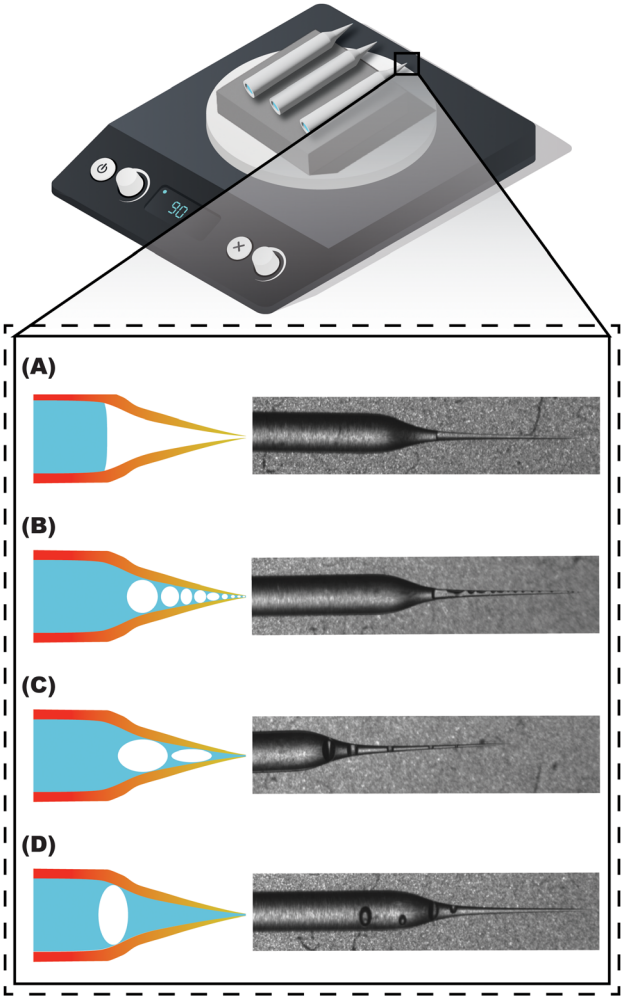

Fig. 4 A schematic of the hot-plate filling method. The nanopipettes are placed on a metal block that is placed on a hot plate. The nanopipettes are positioned so that the taper and the tip extend beyond the heating block (so that it is less directly heated). The hot plate should be set just below the boiling point of the solution to encourage fast vaporization without boiling the solution. (A) shows the unfilled nanopipette taper, which after a few minutes of heating (B) will be filled with unevenly condensed solution and numerous air bubbles. With time, (C) further evaporation and recondensation will merge the air bubbles, and finally (D) a single large air bubble will remain, which can be removed with a syringe.

groups, making them amenable to modification through silane chemistry.[40,41] Silane cross-linkers serve as versatile intermediates that impart reactive surface functionality, enabling subsequent grafting of specialized modifications.[42] Among the various silane options, amine-terminated molecules such as 3-aminopropyltriethoxysilane (APTES) are most commonly employed due to their reactivity and compatibility with diverse downstream chemistries.[43–45]

3.1. Silanization of nanopipettes

Silanization involves the reaction of organosilanes with the silicon oxide nanopipette surface through a kinetically complex process encompassing hydrolysis, condensation, and phase separation steps.[46] Fabrication of a reproducible and uniform silane layer—such as one desirable for the modification of a highly sensitive nanoscale structure—presents significant challenges due to the tendency of silane reagents to self-polymerize, form undesirable oligomeric species and polymers, and interact with surfaces in undesirable ways, including physisorption and non-optimal molecular orientations.[47–49] Silanization reactions are commonly carried out in the liquid-phase, typically utilizing anhydrous solvents such as toluene or ethanol, with the latter solvent being particularly common in literature reports for nanopipette applications.[50] For the silanization of nanopipettes, the aminosilane is typically dissolved at concentrations of 1–5% v/v in ethanol and backfilled into the nanopipette.

Ethanol-based silanization suffers from substantial oligomerization/polymerization if anhydrous conditions cannot be maintained,[51,52] which, in nanopipettes is difficult. While the oligomeric and polymeric by-products that form readily in ethanolic solutions can be easily removed in macroscale substrates by rinsing with acetic acid or methanol, the confined internal geometry of nanopipettes renders this cleaning process ineffective, and cleaning is limited to that undertaken *via* the diffusion of the undesired species out of the nanopipette. Consequently, we have found that ethanol-based silanization often yields suboptimal results characterized by high device-to-device variance, nanopipette blockage, transient desorption of weakly attached silanes during measurements, and mechanical failure including cracking or complete breakage during drying procedures.[50] These problems persist even in relatively large nanopipettes with diameters approaching 500 nm, highlighting the fundamental incompatibility between solution-phase silanization (which is widely and successfully utilized on macro-scale substrates) and nanopipette geometries.

We recommend the silanization of nanopipettes in the vapor-phase, which can circumvent many of the limitations inherent to solution-based approaches.[50] In vapour-phase silanization, the pure liquid silane is placed at the bottom of a desiccator, and the nanopipettes are positioned on the desiccator plate above the liquid (Fig. 5A). Silane vaporization is achieved through the combined application of heating *via* a water bath and through the application of a vacuum using an in-house vacuum tap. Through a 60-minute exposure period, the vaporized silane molecules adsorb onto the nanopipettes, which are transferred to an oven for a 30-minute bake at 110 °C to complete the covalent surface condensation reaction.

Vapor-phase silanization offers several advantages for nanopipette modification. With the absence of backfilling, accidental breakages associated with solution removal, rinsing and handling are minimized. The purity and water content of the silane reagent are also of less importance, since the vapor-phase method naturally selects against oligomerized and polymerized species, as their higher molecular weights and lower vapor pressures limit their evaporation. This selectivity for monomeric silane results in more uniform silane layers that not only provide superior reproducibility (Fig. 5B) in onward

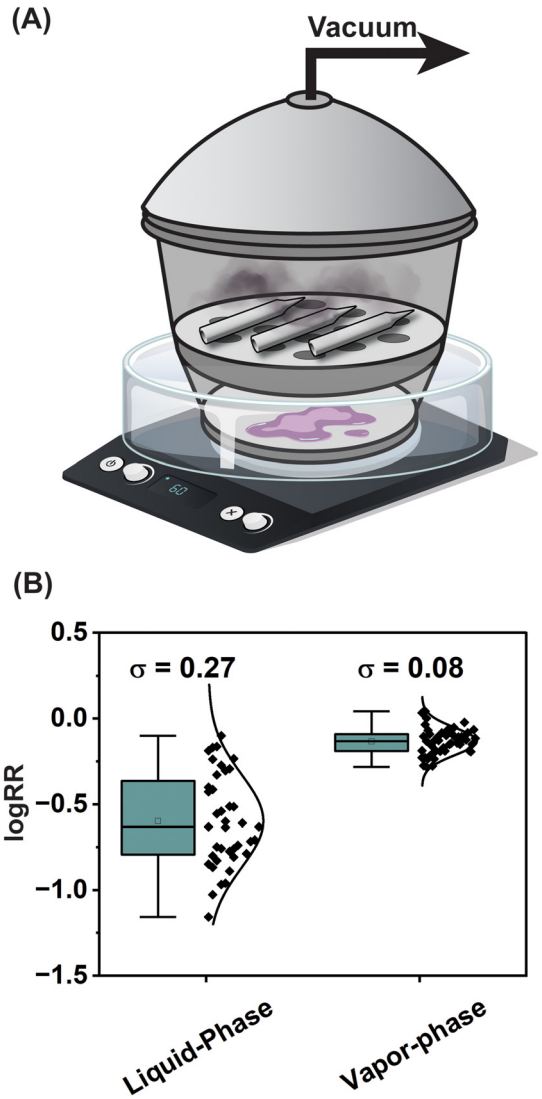

Fig. 5 A schematic of the setup for vapor-phase silanization. (A) 200 μL of the silane is deposed to the bottom of the desiccator in a weighing boat and the nanopipettes are placed on the desiccator plate above the solution. The desiccator is sealed, placed in a 60 °C water bath, and a vacuum is applied using the in-house vacuum tap. Following 60 minutes of vapor exposure, the nanopipettes are oven baked for 30 minutes at 110 °C. (B) compares the reproducibility of the liquid- and vapor-phase silanization methods.

applications but also favorable surface wetting properties that facilitate nanopipette filling. Vapor-phase silanization additionally enables high-throughput nanopipette silanization, with standard desiccators capable of accommodating approximately 80 nanopipettes for simultaneous silanization. The absence of the reactant solution also means that subsequent modification steps can be carried out immediately without the need to clean and dry the nanopipette.

3.2. Designing surface grafting processes for nanopipettes

Most commonly, after silanization, further functionality must be imparted by grafting molecules onto the reactive functionality of the silane cross-linker. This step represents the largest contribution to nanopipette-to-nanopipette variance and is also the primary cause of acute failures, including blockage, de-wetting, cracking, and inability to fill with solution. As the specific molecules that must be immobilized, as well as the required reaction pathway, depend on the intended application, rather than focusing on specific reactions, we will discuss key design principles that should guide the development of the grafting strategy that can prepare functionalized nanopipettes in a practical and highly reproducible manner.

The overarching principle governing the surface modification of nanopipettes is to minimize the amount of cleaning, drying, and solvent exchange. In the nanoconfined tip of a nanopipette, complete removal of unreacted starter reagents and side products is difficult, and the need for solvent exchange and drying steps, as well as the handling associated with these, can result in acute failures, low reproducibility, and low throughput. When designing modification strategies, reaction sequences should be designed to minimize/eliminate the need for cleaning, drying, and changing of solvents. Functionality should be imparted in as few modification steps as possible, with single step grafting representing the ideal scenario. If there is a requirement for complex functionality built in a multi-step assembly, it is strongly preferable to synthesize the complete functional molecule in bulk solution and then immobilize it onto the nanopipette surface in a single grafting step. This approach circumvents the significant challenges associated with multi-step synthesis within the confined nanopipette geometry while maintaining reaction control and enabling proper purification of synthetic intermediates. If multiple reaction steps must be carried out within the nanopipette itself, each step should ideally be performed in the same solvent system, and most preferably in the same solvent that will be used for subsequent electrochemical measurements. This, again, mitigates the need to exchange or remove the previous solvent so that it can be replaced with the solvent of the next reaction step.

When solvent changes are unavoidable, miscible solvents should be employed to enable smooth transitions between reaction steps without the formation of phase boundaries that can trap air bubbles or cause precipitation. Solvent exchange of miscible solvents is generally preferable to oven drying and re-filling, as the latter is more likely to lead to cracking, blockage, or precipitation. The hydrophobicity of intermediate and final surfaces must also be carefully considered throughout the modification process, as surfaces that are too hydrophobic can render nanopipettes completely unfillable with aqueous solutions, effectively terminating the synthetic pathway.

In situations where the ideal single-step, single-solvent approach cannot be implemented and multiple reaction steps, cleaning cycles, and solvent exchanges become necessary, the dip method offers a practical alternative to conventional backfilling procedures. In this approach, modification solutions are not backfilled into the nanopipette; instead, an empty nanopipette, or one filled with a compatible solvent, is simply dipped into the modification solution. The modification solu-

tion penetrates only as far as capillary forces or diffusion allow, creating a smaller reaction volume that can be more efficiently cleaned post-reaction through simple dipping in cleaning solvents. With a smaller reaction volume, solvent exchange is also faster and more thorough. We wish to highlight that the dipping method creates a transition zone between modified and unmodified surfaces within the nanopipette, and this can sometimes cause unusual ion transport behavior. This typically does not compromise the functionality of the nanopipette, as most applications exploit changes in transport properties.

In the case that a silane layer has been deposited prior to further modification (either through solution- or vapor-phase deposition), the temporal aspects of the post-silanization chemistry should also be considered. The reaction immediately succeeding silanization should be fast, as grafting a molecule onto the silane layer stabilizes it and prevents the silane layer's self-hydrolysis and desorption. When the modification reaction proceeds slowly, the silane layer is afforded sufficient time to partially detach from the glass surface, compromising the reproducibility of the overall modification process.[50]

The practical implementation of these principles can be illustrated through a specific example developed within our laboratory. For nanopipette sensors designed to detect trace metal contaminants,[53] we synthesize the analyte-specific probe (a silyl cyclam) in bulk solution, then dissolve the pre-assembled probe in acetonitrile—the same solvent used for subsequent electrochemical characterization. This modification pathway succeeds because it employs a single grafting reaction, avoids drying and refilling procedures, and maintains solvent consistency throughout the process, thereby preventing precipitation of unreacted species.

These considerations collectively form a framework for the design of nanopipette surface modification strategies. While specific applications will dictate the exact surface grafting reaction scheme required, adherence to these principles significantly improves the likelihood of developing robust, reproducible modification protocols that can be successfully implemented across multiple nanopipettes with a high throughput (Fig. 6).

4. Electrochemical characterization of nanopipettes

Once the nanopipettes have been modified and the desired functionality has been imparted, and the nanopipette has been filled with an electrolyte, electrochemical characteriz-

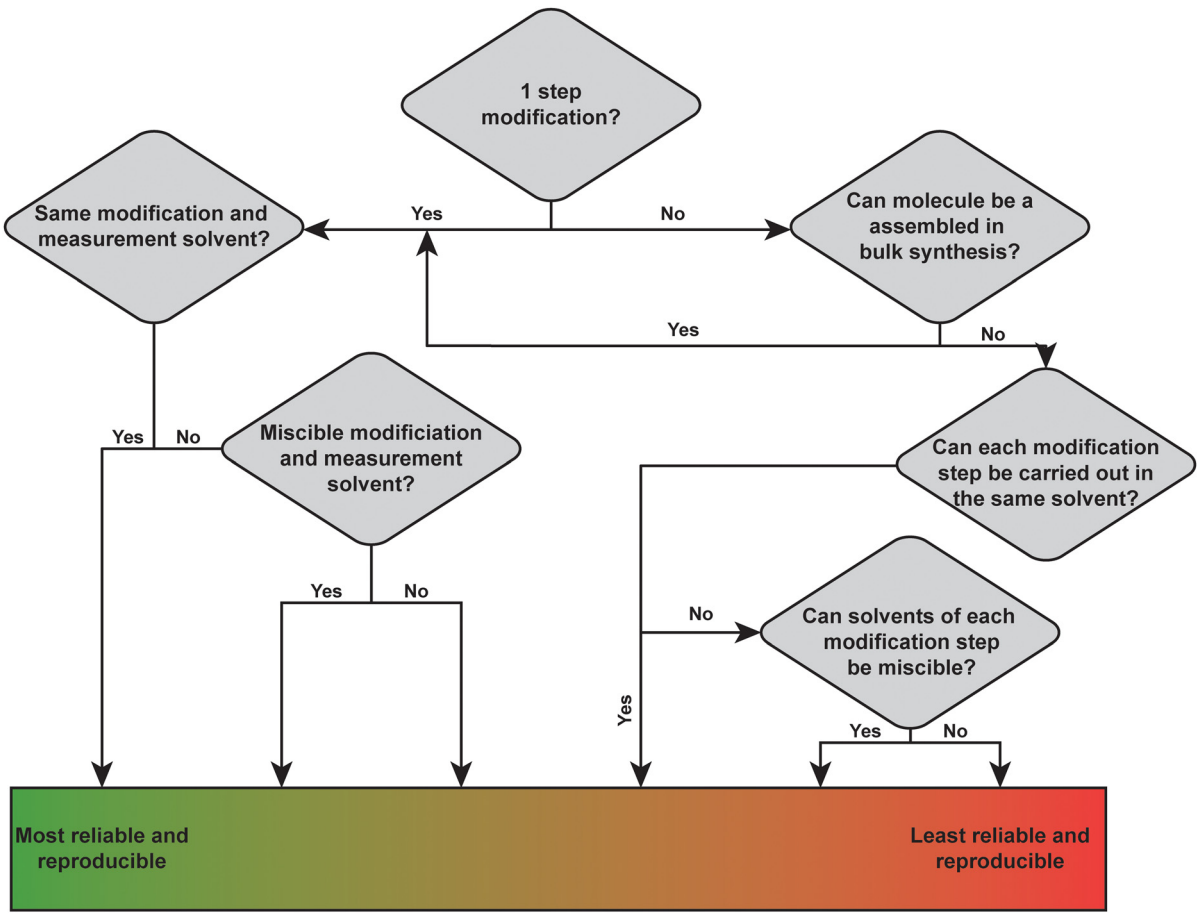

Fig. 6 A flowchart that illustrates the main design choices that will lead to more or less reliable and reproducible surface modification schemes.

ation can take place. An electrochemical cell can be set up using a two-electrode configuration, where the working electrode is placed inside, and the counter/reference electrode outside the nanopipette. The electrodes are usually Ag/AgCl wire electrodes that can be prepared in-house by dipping in bleach for 30 minutes. Platinum wire electrodes can also be used, and are usually more suitable for non-aqueous systems. Current–voltage curves are typically collected between +1 V and −1 V applied potential difference, at scan rates typically ranging from 10 mV s^{-1} to 100 mV s^{-1}.

The nanopipette pore radius can be electrochemically characterized by measuring the conductance in a high electrolyte concentration solution (*i.e.*, 100 mM potassium chloride) where the electric double layers collapse, and the electrochemical response is Ohmic rather than diode-like. The pore conductance is related to the pore radius:[54]

$$r = \frac{G}{\kappa}\left(\frac{1}{\pi \tan\theta} + \frac{1}{4}\right) \quad (1)$$

where r is the pore radius, G is the nanopipette conductance, κ is the solution conductivity, and θ is the nanopipette half-cone angle.

As eqn (1) is only reliable when surface conductance is minimized due to the electric double layer collapse, sizing sub-10 nm nanopipettes can be more challenging. If the electrolyte concentration cannot be further increased, electron microscopy, such as Scanning Transmission Electron Microscopy, remains an alternative. However, even when the electric double layers are overlapping at lower electrolyte concentration, the pore conductance can still be used to screen the nanopipettes for outliers in fabrication and in surface modification. A cracked or broken nanopipette will show higher conductance, while a dewetted/blocked nanopipette will show a lower conductance than average. These outliers can be discarded.

In addition to the pore conductance, the shape of the current–voltage curve should also be used to screen outlier nanopipettes, as well as to diagnose issues. If the pore conductance is normal, but very high rectification is unexpectedly observed, the cause is often chemical contamination, to which nanopipettes, especially unmodified nanopipettes, are extremely sensitive (Fig. 7A). In our experience, cleanliness is incredibly important, and even briefly storing unmodified nanopipettes in a box that has previously stored silanized nanopipettes, or using a contaminated electrode, can cause irreversible contamination. Some current–voltage curves that

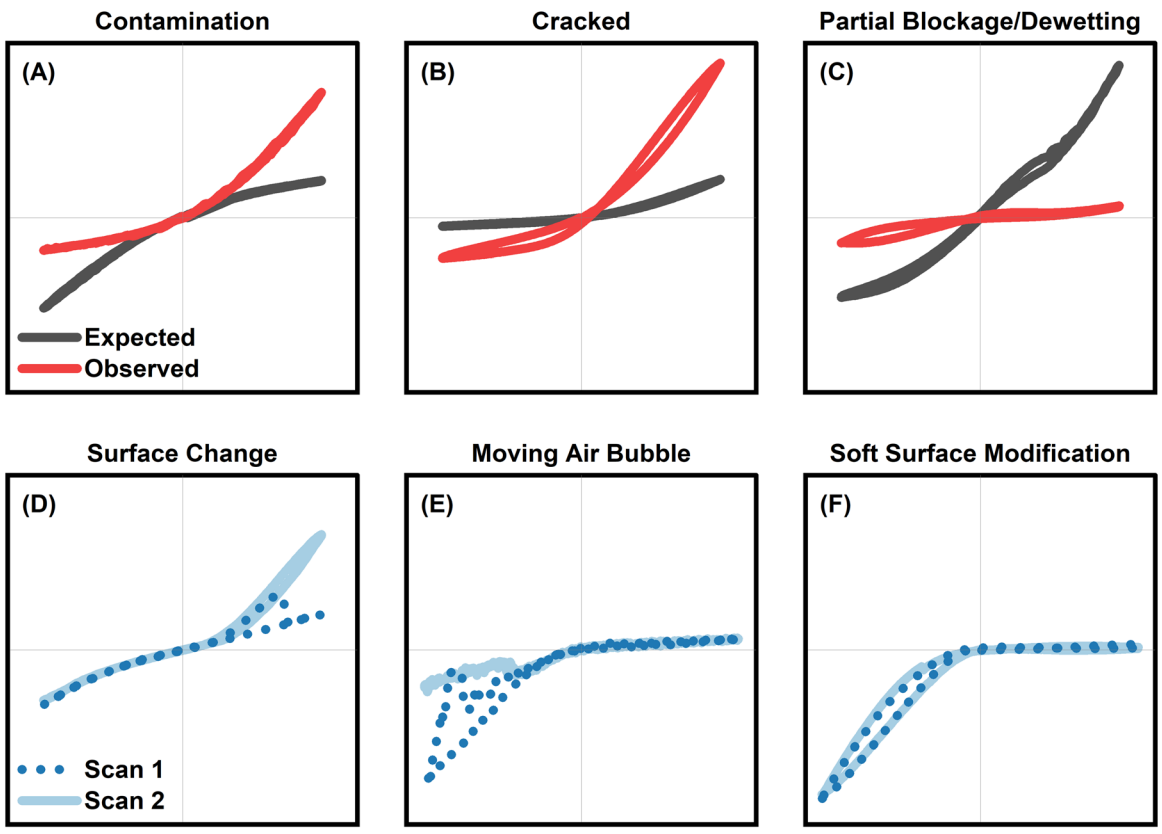

Fig. 7 Current–voltage curves associated with (A) chemical contamination, (B) a crack in the glass wall, (C) partial blockage/dewetting. The grey line represents the expected current–voltage curve. The figure also shows (D) rearrangement/loss of surface functionality mid-scan, (E) a mobile air bubble, and (F) soft and long surface modification (*i.e.* large polymers/DNA).

show a higher conductance, but not so high as to indicate a completely broken off tip, as well as unusual rectification, we associate with the cracking or chipping of the nanopipette (Fig. 7B). A current–voltage curve in which the pore conductance is significantly lower than expected, but rectification is still observed, can be indicative of partial blockage/dewetting, commonly caused by the accumulation or precipitation of surface modifications and reagents (Fig. 7C). This is often observed after a nanopipette is modified, oven-dried, and refilled. Fig. 7D illustrates the loss or shifting of a glob of surface functionality, which suddenly and irreversibly changes the current–voltage curve mid-scan. Current–voltage curves where the pore conductance is low, and there is a sudden increase or decrease in current magnitude at moderate to high applied voltage, are usually indicative of an air bubble in the nanoscale aperture, which moves as the potential is applied (Fig. 7E). These bubbles can sometimes be removed by the application of a large applied voltage while cycling at a fast scan rate. Lastly, current–voltage curves showing high hysteresis are characteristic of soft and flexible surface modifications on the surface (Fig. 7F). Although this is not a fault that should be specifically avoided, it may be undesirable depending on the application. A thorough understanding of the shapes of the current–voltage curves is, however, crucial towards the tuning and optimization of nanopipettes at each of the stages discussed in this perspective, including fabrication, filling, and surface modification.

5. Conclusions

This perspective has highlighted how the practical challenges associated with nanopipette fabrication, filling, silanization, and general surface modification represent a significant barrier for the field, hindering advancement by limiting throughput and reproducibility. Although the unique properties of nanopipettes enable applications such as high-sensitivity single-particle analysis, surface mapping, and localized and bulk analytical measurement, facilitating the advancement of these applications to a high device readiness level requires the practical challenges to be addressed.

The reproducible fabrication of nanopipettes requires environmental control, proper instrument maintenance, and program optimization. While reproducible surface modification strategies should prioritize the minimization of cleaning, drying, and solvent change steps, with single-step grafting reactions maximizing reproducibility and throughput.

Most importantly, these practical challenges are interconnected, with fabrication parameters influencing the filling, the required surface modification scheme dictating handling requirements, and subsequent filling challenges having to be traced back to geometric and chemical issues established at earlier stages. Successfully working with nanopipettes requires a holistic approach where the design of the entire workflow, from initial fabrication through to final measurement, is considered together. This is facilitated by some of the diagnostic current–voltage curves we have offered, which can identify issues associated with each stage of working with nanopipettes.

Although individual laboratories will require specific modifications or alternative approaches for their particular applications and environmental conditions, the general strategies outlined in this perspective are universally applicable and can guide the development of a workflow, enabling researchers, established and new alike, to advance the field of nanopipettes with higher throughput and more reliable measurements.

Author contributions

DD: conceptualization, visualization, writing (original draft, review & editing). AMA: writing (review & editing). RPJ: conceptualization, writing (review & editing), supervision.

Conflicts of interest

There are no conflicts to declare.

Data availability

No primary research results, software, or code have been included, and no new data were generated or analysed as part of this perspective.

Acknowledgements

We acknowledge funding from Health Research Board under the JPIAMR Joint Transnational Call (Project No. JPI-AMR-2023-1) and from Science Foundation Ireland under the Frontiers for the Future Programme (20/FFP-P/8728). DD acknowledges postgraduate scholarship funding from the Irish Research Council (Project No. GOIPG/2022/1648).

References

1 S. Zhang, W. Chen, L. Song, X. Wang, W. Sun, P. Song, G. Ashraf, B. Liu and Y.-D. Zhao, *Sens. Actuator Rep.*, 2021, 100042.
2 D. Duleba and R. P. Johnson, *Curr. Opin. Electrochem.*, 2022, **34**, 100989.
3 W. Si, J. Sha, Q. Sun, Z. He, L. Wu, C. Chen, S. Yu and Y. Chen, *Analyst*, 2020, **145**, 1657–1666.
4 L. Yang and T. Yamamoto, *Front. Microbiol.*, 2016, **7**, 1500.
5 R. Maugi, P. Hauer, J. Bowen, E. Ashman, E. Hunsicker and M. Platt, *Nanoscale*, 2020, **12**, 262–270.
6 C. C. Harrell, Y. Choi, L. P. Horne, L. A. Baker, Z. S. Siwy and C. R. Martin, *Langmuir*, 2006, **22**, 10837–10843.
7 M. Wanunu, *Phys. Life Rev.*, 2012, **9**, 125–158.

8 J. Wei, H. Hong, X. Wang, X. Lei, M. Ye and Z. Liu, *Nanoscale*, 2024, **16**, 18732–18766.
9 S. Howorka, *Nat. Nanotechnol.*, 2017, **12**, 619–630.
10 M. Ayub and H. Bayley, *Curr. Opin. Chem. Biol.*, 2016, **34**, 117–126.
11 L. Xue, H. Yamazaki, R. Ren, M. Wanunu, A. P. Ivanov and J. B. Edel, *Nat. Rev. Mater.*, 2020, **5**, 931–951.
12 K. Lee, K.-B. Park, H.-J. Kim, J.-S. Yu, H. Chae, H.-M. Kim and K.-B. Kim, *Adv. Mater.*, 2018, **30**, 1704680.
13 Q. Chen and Z. Liu, *Sensors*, 2019, **19**, 1886.
14 T. Ma, J.-M. Janot and S. Balme, *Small Methods*, 2020, **4**, 2000366.
15 J. P. Fried, J. L. Swett, B. Paulose Nadappuram, J. A. Mol, J. B. Edel, A. P. Ivanov and J. R. Yates, *Chem. Soc. Rev.*, 2021, **50**, 4974–4992.
16 J. Stanley and N. Pourmand, *APL Mater.*, 2020, **8**, 100902.
17 S. Zhang, M. Li, B. Su and Y. Shao, *Annu. Rev. Anal. Chem.*, 2018, **11**, 265–286.
18 C. A. Morris, A. K. Friedman and L. A. Baker, *Analyst*, 2010, **135**, 2190–2202.
19 A. J. Bard, F.-R. F. Fan, D. T. Pierce, P. R. Unwin, D. O. Wipf and F. Zhou, *Science*, 1991, **254**, 68–74.
20 C. Zhu, K. Huang, N. P. Siepser and L. A. Baker, *Chem. Rev.*, 2020, **121**, 11726–11768.
21 P. K. Hansma, B. Drake, O. Marti, S. A. C. Gould and C. B. Prater, *Science*, 1989, **243**, 641–643.
22 A. Saha-Shah, A. E. Weber, J. A. Karty, S. J. Ray, G. M. Hieftje and L. A. Baker, *Chem. Sci.*, 2015, **6**, 3334–3341.
23 S.-M. Lu and Y.-T. Long, *TrAC, Trends Anal. Chem.*, 2019, **117**, 39–46.
24 G. Bulbul, G. Chaves, J. Olivier, R. E. Ozel and N. Pourmand, *Cells*, 2018, **7**, 55.
25 M. Chang, G. Morgan, F. Bedier, A. Chieng, P. Gomez, S. Raminani and Y. Wang, *J. Electrochem. Soc.*, 2020, **167**, 037533.
26 Y. Wang, D. Wang and M. V. Mirkin, *Proc. R. Soc. A*, 2017, **473**, 20160931.
27 Y. Wang, K. Kececi, M. V. Mirkin, V. Mani, N. Sardesai and J. F. Rusling, *Chem. Sci.*, 2013, **4**, 655–663.
28 Z. Siwy, E. Heins, C. C. Harrell, P. Kohli and C. R. Martin, *J. Am. Chem. Soc.*, 2004, **126**, 10850–10851.
29 Z. Siwy and A. Fuliński, *Am. J. Phys.*, 2004, **72**, 567–574.
30 I. Vlassiouk, T. R. Kozel and Z. S. Siwy, *J. Am. Chem. Soc.*, 2009, **131**, 8211–8220.
31 D. Woermann, *Phys. Chem. Chem. Phys.*, 2003, **5**, 1853–1858.
32 K. Shigyou, L. Sun, R. Yajima, S. Takigaura, M. Tajima, H. Furusho, Y. Kikuchi, K. Miyazawa, T. Fukuma, A. Taoka, T. Ando and S. Watanabe, *Anal. Chem.*, 2020, **92**, 15388–15393.
33 C. W. Leasor, K. L. Vernon, Y. Wang, R. E. Baker and L. A. Baker, *Anal. Methods*, 2025, **17**, 5973–5981.
34 L. Sun, K. Shigyou, T. Ando and S. Watanabe, *Anal. Chem.*, 2019, **91**, 14080–14084.
35 X. Su, M. L. Yusuf, X. Guo, J. Liu, S. Fan, S. Li, H. Li and F. Xia, *Anal. Chem.*, 2025, **97**, 10503–10520.
36 L. Ao-Xue, Y. Dan, L. Hong-Na, L. Guo-Hui, F. Qiang, S. Yu-Ping, Y. Guo-Cheng and H. Jin, *Chin. J. Anal. Chem.*, 2019, **47**, e19081–e19087.
37 H. Wang, H. Tang, X. Qiu and Y. Li, *Chem. – Eur. J.*, 2024, **30**, e202400281.
38 P. Actis, A. C. Mak and N. Pourmand, *Bioanal. Rev.*, 2010, **1**, 177–185.
39 S. Denuga, D. Duleba, P. Dutta, G. Macori, D. K. Corrigan, S. Fanning and R. P. Johnson, *Sens. Diagn.*, 2024, **3**, 1068–1075.
40 G. L. Witucki, *J. Coat. Technol. Res.*, 1993, **65**, 57–60.
41 S. Onclin, B. J. Ravoo and D. N. Reinhoudt, *Angew. Chem., Int. Ed.*, 2005, **44**, 6282–6304.
42 N. S. K. Gunda, M. Singh, L. Norman, K. Kaur and S. K. Mitra, *Appl. Surf. Sci.*, 2014, **305**, 522–530.
43 M. Hijazi, V. Stambouli, M. Rieu, V. Barnier, G. Tournier, T. Demes, J.-P. Viricelle and C. Pijolat, *J. Mater. Sci.*, 2018, **53**, 727–738.
44 M. Antoniou, D. Tsounidi, P. S. Petrou, K. G. Beltsios and S. E. Kakabakos, *Med. Devices Sens.*, 2020, **3**, e10072.
45 A. Miranda, L. Martínez and P. A. A. De Beule, *MethodsX*, 2020, **7**, 100931.
46 A. A. Issa and A. S. Luyt, *Polymers*, 2019, **11**, 537.
47 E. Asenath Smith and W. Chen, *Langmuir*, 2008, **24**, 12405–12409.
48 A. R. Yadav, R. Sriram, J. A. Carter and B. L. Miller, *Mater. Sci. Eng., C*, 2014, **35**, 283–290.
49 V. G. P. Sripathi, B. L. Mojet, A. Nijmeijer and N. E. Benes, *Microporous Mesoporous Mater.*, 2013, **172**, 1–6.
50 D. Duleba, S. Denuga and R. P. Johnson, *Phys. Chem. Chem. Phys.*, 2024, **26**, 15452–15460.
51 M. E. McGovern, K. M. Kallury and M. Thompson, *Langmuir*, 1994, **10**, 3607–3614.
52 S. Fiorilli, P. Rivolo, E. Descrovi, C. Ricciardi, L. Pasquardini, L. Lunelli, L. Vanzetti, C. Pederzolli, B. Onida and E. Garrone, *J. Colloid Interface Sci.*, 2008, **321**, 235–241.
53 E. B. Farrell, F. McNeill, A. Weiss, D. Duleba, P. J. Guiry and R. P. Johnson, *Anal. Chem.*, 2024, **96**, 6044–6064.
54 D. Perry, D. Momotenko, R. A. Lazenby, M. Kang and P. R. Unwin, *Anal. Chem.*, 2016, **88**, 5523–5530.

